Bull. Astr. Soc. India (2013) **41**, 209–226

Photometric study of Galactic open cluster NGC 2129, NGC 1502 and King 12

A. Tripathi[1]*, U. S. Pandey[1]† and Brijesh Kumar[2]‡

[1]*Department of Physics, Deen Dayal Upadhyaya Gorakhpur University, Gorakhpur, Uttar Pradesh 273009, India*

[2]*Aryabhatta Research Institute of Observational Sciences, Manora Peak, Nainital 263129, India*

Received 2013 April 02; accepted 2013 September 23

Abstract. We present deep Johnson UBV and Cousins RI CCD photometry of three young open clusters, namely, NGC 2129, NGC 1502 and King 12 reaching down to V ∼ 22 mag. For the first time, we have reported optical CCD data for King 12. Fundamental parameters for these clusters have been determined by comparing colour-colour and colour-magnitude diagrams (CMDs) with the theoretical models. The cluster radii have been estimated to be 3.3, 1.7 and 3.9 pc for NGC 2129, NGC 1502 and King 12 respectively. The reddenings E(B-V) have been determined to be 0.77±0.05, 0.68±0.05 and 0.63±0.05 while the corresponding distances have been found to be 2.1±0.1, 1.0±0.1 and 2.5±0.1 kpc respectively. The ages of the clusters have been obtained after fitting theoretical stellar evolutionary models for solar metallicity Z = 0.019 isochrones with the observed CMDs. This gives an age of 10.0±0.1 Myr for all the three clusters. The analysis shows that there is differential interstellar reddening in the direction of all clusters.

Keywords : Hertzsprung-Russell (HR) diagram – open clusters and associations: individual: NGC 2129, NGC 1502 and King 12

1. Introduction

Open clusters (OCs) are valuable probes for investigations of Galactic disc properties. For example, the color-magnitude diagrams (CMDs) of OCs help us to obtain fundamental parameters

*email: aparatrip@gmail.com

†email: uspandey@aries.res.in

‡email: brij@aries.res.in

such as reddening, distance and age. Furthermore, these parameters are also used to constrain theoretical models for the structure, dynamical evolution and star formation process in the Galaxy (Yadav et al. 2008) in general and the Galactic disc in particular.

In an earlier study of OCs, Subramaniam & Bhatt (2007) examined the distribution of clusters with different ages in the outer Galactic disk between l=90° and 135° and report evidence of a mild warp (see also (Carraro, Chaboyer & Perencevich 2006; Subramaniam, Carraro & Janes 2010)). In fact, these studies are significant for understanding the structure and dynamical evolution of the Galactic disc. In the present work, we therefore select OCs NGC 2129, NGC 1502 and King 12 as target objects.

Brief details about these three clusters are summarized below.

NGC 2129: It is located in the Gemini Constellation about 2 degrees south-west of the more conspicuous OC M35 and NGC 2158 towards the Galactic anti-centre. CCD photometry has been done by Carraro et al. (2006). They estimated the radius of the cluster to be between 2.0 - 2.5 arcmin and being 2200 pc away from the Sun in the anti-center direction inside the local spiral arm, with a mean reddening of E(B-V)=0.82 and an age of approximately 10 Myr.

NGC 1502: It is located in the northern hemisphere and is a highly reddened open cluster in the outer border of the Orion spiral arm. Several photometric studies have been done by Purgathofer (1961); Reimann & Pfau (1987); Tapia et al. (1991); Delgado et al. (1992); Crawford (1994). The age of the cluster has been found to be 10 Myr, the reddening to be E(b-y) = 0.54 mag and its distance to be 960 ± 25pc.

King 12: Haug (1970) obtained photometric magnitudes of three stars in the cluster field. Mohan & Pandey (1984) obtained photoelectric magnitudes of 30 stars and estimated its age to be between the NGC 2362 and NGC 884 groups and its distance as 2.49 kpc. They reported variability in reddening across the field. No CCD photometric studies are available for King 12.

Johnson UBV and Cousins RI CCD photometry provide a valuable tool to obtain fundamental parameters of OCs. We aim to report here high quality CCD photometric data down to V∼22 mag in three Galactic fields used to determine their fundamental parameters like reddening, distances, and ages. Table 1 lists the relevant information available for these as given in the Dias et al. (2002) catalogue.

Table 1. Fundamental parameters of the clusters taken from the Dias et al. catalogue.

Cluster	α_{J2000}	δ_{J2000}	l	b	size	E(B-V)	Dist.	Age
	h:m:s	d:m:s	(°)		(′)	mag	(kpc)	(log)
NGC 2129	06:00:41	+23:19:06	186.555	0.056	2.5	0.8	2.2	7.000
NGC 1502	04:07:50	+62:19:54	143.672	7.658	4.0	0.70	1.0	7.000
King 12	23:53:00	+61:58:00	116.124	-0.130	1.5	0.59	2.4	7.037

The layout of the paper is as follows. A brief description of the observations, data reduction procedures and photometric comparisons are presented in Section 2; data analyses including reddening, CMDs, ages and distances to the clusters are presented in Section 3. The results are summarized in Section 4.

2. Observations and data reduction

Observations for all three clusters in the Johnson UBV and Cousins RI bands were taken using 104-cm Sampurnanand reflector telescope of Aryabhatta Research Institute of Observational Sciences, Nainital, during the period of November-December 2004. The CCD camera used is thinned back-illuminated and mounted at f/13 Cassegrain focus. Images were recorded using 24 μm square sized pixels in a 2048×2048 sized CCD detector which corresponds to 0.38 arcsec and covers 13×13 arcmin^2 on the sky. Binned mode of 2×2 pixels is used during observations to improve the signal-to-noise ratio. The readout noise for the CCD is 5.3 electrons with a gain factor of 10 electrons per ADU. The observing log is given in Table 2.

To clean the images, number of bias and twilight flat-field frames were taken in all the filters. Multiple short and long exposures have been obtained for all three clusters. To calibrate the magnitude of stars in cluster field, standard field SA98 of Landolt (1992) were also observed. Airmass used for extinction determinations, covers the range of 1.15 to 2.13 for Landolt (1992) standards. The spread in the Point Spread Function (PSF) caused by seeing can be approximated by a central Gaussian and the large outer part by a power law. A commonly used measure for the angular size of the PSF is the diameter where the flux falls to half its central value, i.e, full width at half maxima (FWHM). The mean Gaussian FWHM of the stellar images varied from about 2.5 to 5.0 pixel (see Table 2). The standard field covers a range in brightness (10.9<V<17.3) as well as in color (0.16<(B-V)< 1.91).

Data reduction was done using computing facilities available at ARIES, Nainital. IRAF/ MIDAS data reduction package has been used for initial processing of data frames which includes bias subtraction, flat fielding and cosmic ray removal. Photometry of bias-subtracted and flat fielded CCD frames was carried out using DAOPHOT -II software (Stetson 1987, 1992). To obtain quantitative values for the brightness of stars aperture photometry and profile fitting photometry was done. 22 isolated bright stars were selected to get a profile fitting function. The obtained PSF was applied to all the stars with the help of ALLSTAR routine of DAOPHOT II. We used DAOGROW program for construction of an aperture growth curve required for determining the difference between aperture and profile fitting magnitude. These aperture corrected magnitudes are applied to the PSF magnitudes to get the aperture instrumental magnitudes. For cross-identification of the stars measured on different frames of the cluster DAOMASTER program was used. Magnitudes of bright stars saturated in deep exposure frames were taken from short-exposure frames. For translating the observed aperture magnitudes to the standard magnitudes least-square linear regressions outlined by Stetson (2000) were fitted. The following calibration equations were derived:

Table 2. Log of observations, with dates and exposure times for each passband.

Cluster	Date (Year 2004)	filter	Exp (sec)	Airmass	FWHM (pixel)
NGC 2129	Dec 03	V	900×3	1.07-1.18	3.17-3.56
		R	600×3	1.23-1.32	3.37-3.54
		I	300×3	1.38-1.45	3.38-3.61
	Dec 05	U	1800×2,1200×1	1.01-1.07	2.90-3.22
		B	1200×3	1.01-1.01	2.79-3.23
	Dec 12	U	300×2	1.01-1.01	2.69-2.62
		B	300×2	1.01-1.01	2.83-2.81
		V	240×2	1.01-1.01	2.83-2.75
		R	180×2	1.01-1.01	2.69-2.75
		I	120×2	1.02-1.02	2.64-2.60
SA98	Dec 12	U	300×5	1.15-1.83	3.08-4.76
		B	240×5	1.15-1.90	3.40-4.60
		V	240×5	1.15-1.97	2.91-4.58
		R	120×5	1.16-2.06	2.61-4.70
		I	60×5	1.16-2.13	2.63-4.27
NGC 1502	Dec 01	U	1800×3	1.19-1.21	2.45-4.11
		B	1200×2	1.23-1.25	2.48-2.48
		V	600×3	1.21-1.24	2.50-2.64
		R	600×3	1.26-1.29	2.57-2.69
		I	300×3	1.31-1.33	2.49-2.65
	Dec 12	U	300×2	1.23-1.24	4.43-4.90
		B	240×2	1.24-1.25	4.56-4.78
		V	180×2	1.25-1.26	3.87-3.88
		R	120×2	1.27-1.28	3.49-3.71
		I	80×2	1.29-1.28	4.05-3.85
King12	Nov 16	B	1200×3	1.32-1.42	3.51-3.70
		V	900×3	1.19-1.20	3.43-4.05
		R	480×3	1.19-1.20	3.39-3.64
		I	300×3	1.21-1.22	3.20-3.53
	Dec 04	U	1800×2	1.25-1.29	3.43-3.46
	Dec 12	U	300×2	1.24-1.25	3.93-4.26
		B	240×2	1.23-1.23	3.72-3.90
		V	180×2	1.22-1.22	3.61-3.66
		R	120×2	1.21-1.21	3.10-3.51
		I	60×2	1.20-1.21	2.92-3.19

$v = V + 4.26 \pm 0.01 - (0.04 \pm 0.01)(B - V) + (0.15 \pm 0.01)X$
$b = B + 4.67 \pm 0.01 - (0.04 \pm 0.01)(B - V) + (0.27 \pm 0.01)X$
$i = I + 4.69 \pm 0.01 - (0.05 \pm 0.01)(V - I) + (0.07 \pm 0.01)X$
$r = R + 4.16 \pm 0.01 - (0.04 \pm 0.01)(V - R) + (0.12 \pm 0.01)X$
$u = U + 6.87 \pm 0.01 - (0.03 \pm 0.01)(U - B) + (0.51 \pm 0.03)X$

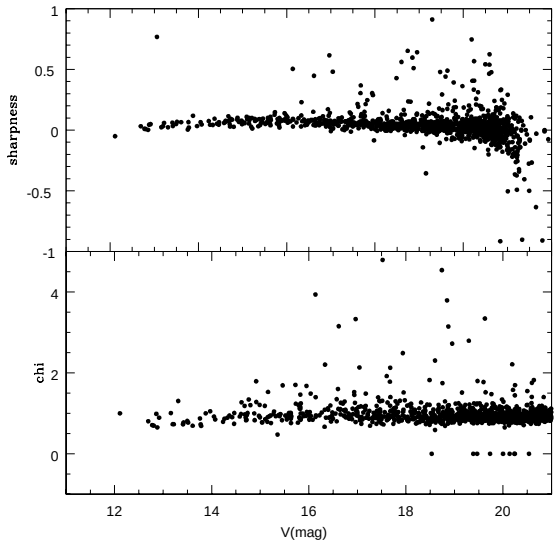

Figure 1. Image parameter χ and sharpness as a function of V magnitude.

where V, B, I, R and U are the standard magnitudes and v, b, i, r, u are the instrumental aperture magnitudes normalized for 1 sec of exposure time and X is the airmass. Second order colour correction terms are small in comparison with the other photometric data reduction errors; so these have been ignored. Zero-points for local standards were evaluated taking account of the aperture growth curve, difference in exposure times and atmospheric extinction. The errors in zero-points and colour coefficients are ∼0.01 mag. We took 16 standard stars of Landolt (1992) and 12 standard stars of Stetson (2000) from the observed field of SA98. The rms deviations of the Landolt and Stetson standards around the fitted magnitudes were found to be ∼0.03 mag in UBVRI bands.

A final catalogue of stellar objects identified in at least two filters were obtained with shape-defining parameters $0.2 \leq$ sharpness < 1.0 and goodness of fit estimator $\chi < 5$ as shown in Fig. 1.

The accuracy of the morphology and position of the cluster features in CMDs depends on the variation of photometric errors with magnitudes. Photometric errors are approximated to be related with the signal-to-noise ratio of the source. ALLSTAR evaluates the error as the mean square root of the residuals of the fittings of a PSF to the profile of the central part of each star. The internal errors as derived from DAOPHOT in U, B, V, R and I are plotted against V mag in Fig. 2. This shows that the photometric errors are less than 0.01 mag at V∼18 mag in B, less than 0.01 mag at V∼19 mag in V, R bands.

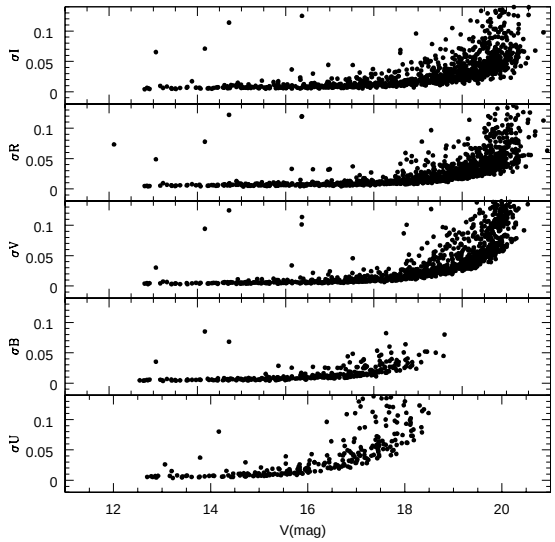

Figure 2. The photometric errors corresponding to the brightness measurements at U, B, V, R, and I are plotted against the V-band brightness. Errors on the y-axis represent the internal error as estimated by DAOPHOT routine.

The basic step to provide the celestial coordinates of all the stars in J2000.0 is to get the astrometric solution. To obtain this solution, we used the SkyCat tool. We found 10 bright stars per field for which we have both the celestial coordinates and the corresponding pixel coordinates. Then by using IRAF task CCMAP and CCTRAN, we found the corresponding transformation between the two coordinate systems and computed the individual celestial coordinates for all the detected stars. The transformations have an r.m.s. value of about 0.06″ in RA and DEC. These are available only in electronic form.

2.1 Comparison with previous photometry

Comparison of present CCD data with that available photoelectric (Hoag et al. 1961) and CCD photometry (Carraro et al. 2006) have been done for the cluster NGC 2129. In Fig. 3, difference (present data – Hoag et al. (1961) data) ΔV, Δ(B-V) and Δ(U-B) with V magnitudes have been plotted. Fig. 4 shows difference between present data and Carraro et al. (2006) in ΔV, ΔB, ΔI, ΔR, ΔU with V and (B-V). Comparing on a star-by-star basis 38 stars were found to be in common with the photoelectric data of Hoag et al. (1961) and 159 stars with that of the CCD photometric data given by Carraro et al. (2006). Fig. 4 indicates a zero point offset ~ 0.02 mag in V whereas ~0.1 mag B, I, R and U. Bright stars HD 250289 and 250290 are saturated in our CCD photometry. We took photometric data from Carraro et al. (2006) for those stars which have saturated in our photometry but not in the photometry of Carraro et al. (2006). Fig. 4 shows that the distribution of photometric differences seems fairly random with a constant zero-point offset,

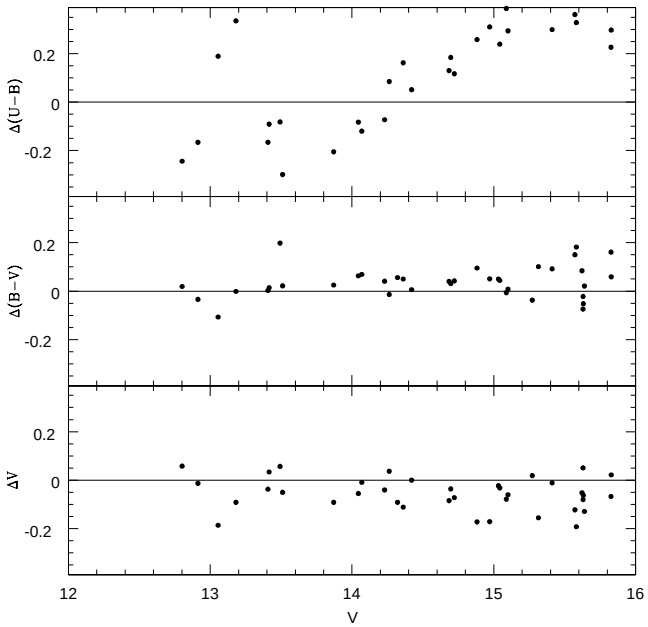

Figure 3. Comparison between the present photometry in NGC 2129 with that of Hoag et al. (1961). The differences Δ V, Δ (B-V) and Δ (U-B) denote deviations of present photometry from the Hoag et al. data.

except for few outliers, which appear to be mostly stars that were treated as single. However, blending in light of stars might affect the system in cases of doubles. We note an increase in the scatter with decreasing brightness and it becomes more than ∼0.1 mag at fainter levels. As in the case of Carraro et al. (2006), we also notice a colour term effect in particularly U band.

3. Analysis of the data

3.1 Profile and cluster radius

Cluster radius r_c is taken as the distance from the cluster center to where the average cluster contribution becomes negligible with respect to the background stellar field. Cluster radius as well as extent of field-star contamination is estimated using spatial surface density profile of stars. As shown in Table 1, the diameters of all three clusters are less than the field observed so our photometry covers entire cluster field. For quantitative estimation of the cluster size we took eye estimated cluster center. The cluster region has been divided into a number of concentric circles with an annulus of width 36 arcsec. Star counts are carried out in concentric rings around the cluster center and are then divided by the respective areas. Poisson errors have also been derived and normalized to the corresponding area. The projected radial stellar density is plotted in Fig. 5b, 7b and 9b for all three clusters for two magnitude ranges V<15 and V<17. The error

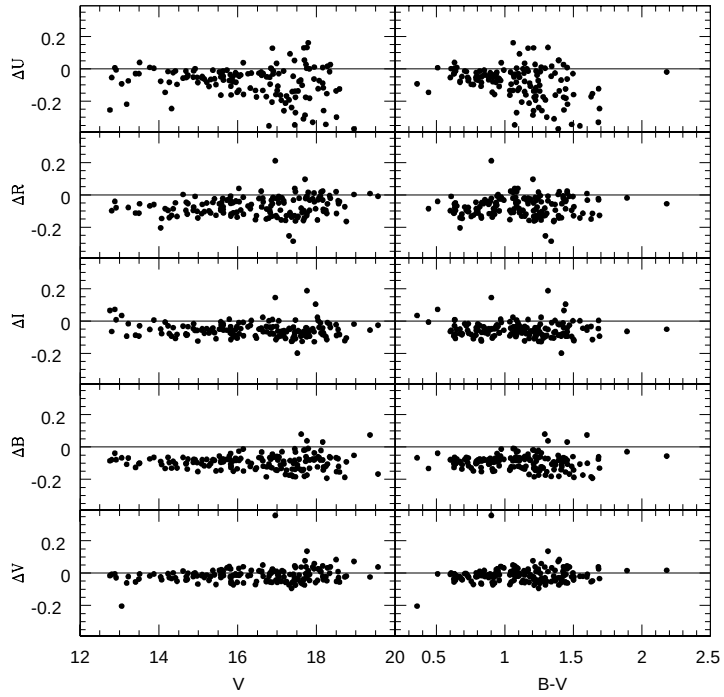

Figure 4. Comparison between our photometry in NGC 2129 with those of Carraro et al. (2006). The differences ΔV, ΔB, ΔI, ΔR and ΔU denote deviations of present photometry from Carraro et al. (2006) data.

bars denote the Poisson statistics. 2MASS K-band data have been used to support the radial density profile fits.

In Fig. 5b, for V<17 for NGC 2129, logarithmic density of stars per unit area for radii ≥ 3 arcmin goes approximately to zero and for V < 15, it goes to -0.5. Density profile is decreasing and flattens at around 3.3 arcmin. Therefore, 3.3 arcmin (3.3 pc) has been considered to be the cluster radius, which is slightly larger than the value listed in Table 1.

Fig. 7b shows that the radius is slightly larger than the value listed in Table 1. The radial density profile for NGC 1502 decreases and reaches the level of the field at about 3.7 arcmin (1.7 pc). This has been adopted as the radius of the cluster. This value of radius is slightly lower than the value given in Table 1.

In the case of King 12 (Fig. 9b), for V<17 logarithmic density of stars per unit area for radii ≥ 3 arcmin goes approximately to 0.3 and for V<15, it goes to −0.4. The radial density profile is

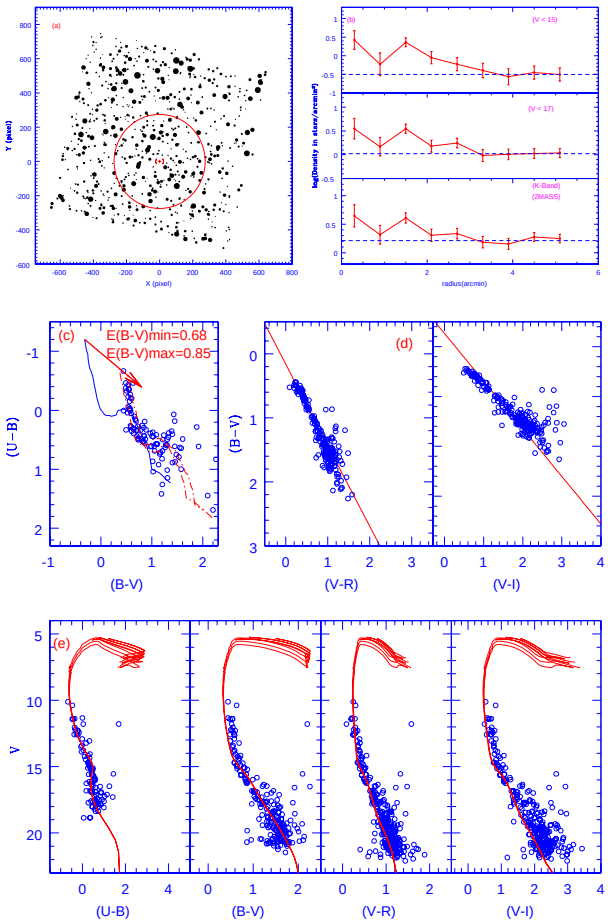

Figure 5. NGC 2129. (a) Identification chart for the observed region of NGC 2129. Filled circles represent apparent magnitude such that brighter stars have larger sizes. The ring defines the cluster boundary. (b) Surface density of stars around the cluster center. Poisson errors are shown with vertical bars. (c) The color-color diagram for the cluster region ($r < r_c$). The (U-B) versus (B-V) diagrams of the stars in cluster region. Continuous straight line represents slope of the reddening vector. Solid line is the Schmidt-Kaler (1982) empirical ZAMS, whereas the dashed lines are the same ZAMS, but shifted by E(B-V) = 0.68 and 0.85 respectively. (d) It shows (V-R)/(B-V) and (V-I)/(B-V) color-color diagram for stars taken within cluster region. The straight line shows least-square fit to the data. (e) The CMDs for the cluster region ($r < r_c$). Isochrones from Girardi et al. (2002) confining the best age estimations are shown by dashed and solid continuous curve for log(age) = 6.95, 7.00 and 7.05.

smooth and flattens around 2.7 arcmin (3.9 pc) and begins to merge with the background stellar density. Therefore, 2.7 arcmin has been taken as the cluster radius. This estimate is much larger than the value listed in Table 1.

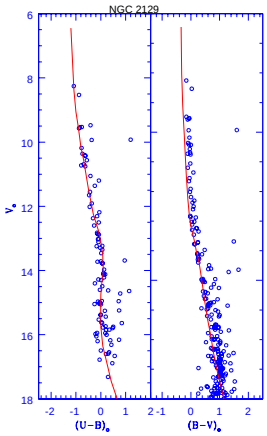

Figure 6. $V_o/(U\text{-}B)_o$ and $V_o/(B\text{-}V)_o$ CMD of stars lying within the cluster region of the cluster NGC 2129. Solid line is the Schmidt-Kaler (1982) shifted by distance modulus of 11.65 mag.

3.2 Color magnitude diagrams

Colour magnitude diagrams are used to estimate the cluster fundamental parameters such as age, distance etc. For proper analysis of the CMDs of the clusters, it is necessary to distinguish the cluster sequence from the field-star contamination. Therefore CMDs of stars outside the cluster radius have also been constructed. The V/(U-B); V/(B-V); V/(V-R) and V/(V-I) colour-magnitude diagrams of the cluster ($r < r_c$) region along with V/(B-V) CMD ($r > r_c$) of the field region are shown in the Figs. 5e, 7e, 9e and 11 for clusters NGC 2129. NGC 1502 and King 12 respectively. The morphology of the CMDs implies that all three clusters are of young-age.

NGC 2129: For NGC 2129, the main-sequence extends from V$\sim$ 10 mag to V$\sim$ 22 mag. It is seen that the field star contamination becomes more evident for stars V > 18 mag. Therefore stars under the cluster radius (r < 3.3 arcmin) have been considered for the CMDs.

NGC 1502: For NGC 1502, the main-sequence extending from V$\sim$7 to V$\sim$22 mag is visible in V, (B-V) in CMD. The main- sequence has more scatter and field contamination in the fainter part V > 17 mag of the CMDs.

King 12: A characteristic main-sequence from V$\sim$9.8 to V$\sim$22 mag is seen in V, (B-V) CMD. The scatter is more prominent for V > 15 mag.

CMDs of OCs are dominated by contamination due to background population. Stars to the left of the ZAMS line in the cluster CMD are considered as field stars. Stars lying to the right of ZAMS line may be either field stars or pre-main-sequence stars (PMS). We have therefore plotted PMS isochrones using data given by Siess, Dufour & Forestini (2000) for different ages as shown

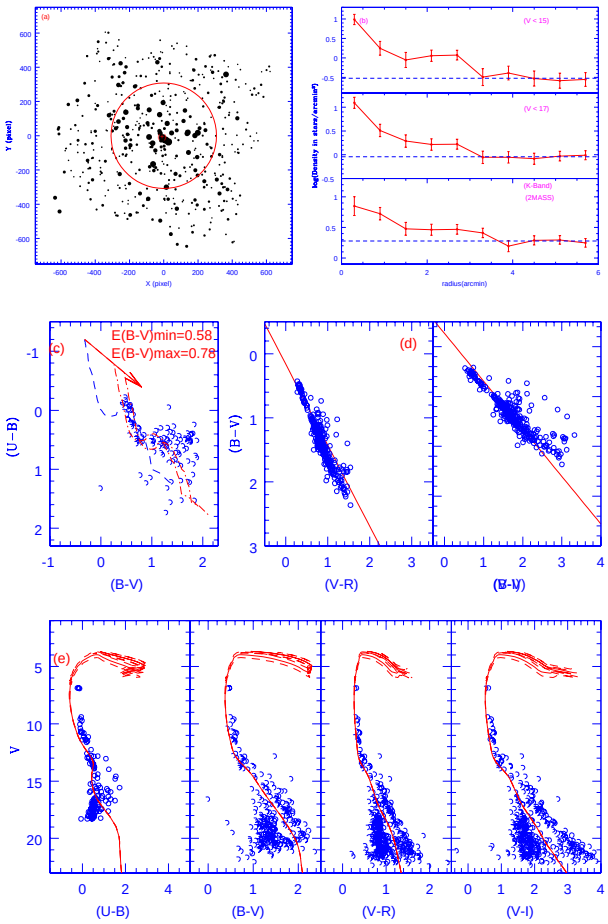

Figure 7. NGC 1502. (a) Identification chart for the observed region of NGC 1502. Filled circles represent apparent magnitude such that brighter stars have larger sizes. The ring defines the cluster boundary. (b) Surface density of stars around the cluster center. Poisson errors are shown with vertical bars. (c) The color-color diagram for the cluster region ($r < r_c$). The (U-B) versus (B-V) diagrams of the stars in cluster region. Continuous straight line represents slope of the reddening vector. Solid line is the Schmidt-Kaler (1982) empirical ZAMS, whereas the dashed lines are the same ZAMS, but shifted by E(B-V) = 0.58 and 0.78 respectively. (d) It shows (V-R)/(B-V) and (V-I)/(B-V) color-color diagram for stars taken within cluster region. The straight line shows least-square fit to the data. (e) The CMDs for the cluster region ($r < r_c$). Isochrones from Girardi et al. (2002) confining the best age estimations are shown by dashed and solid continuous curve for log(age) = 6.95, 7.00 and 7.05.

by Fig. 12a for NGC 2129, Fig. 12b for King 12 and Fig. 13 for NGC 1502. We compare CMDs of stars lying within the region $r < r_c$ for all three clusters. We note that in clusters NGC 2129 and King 12, there is scarcity of stars between the age 2 - 10 Myr. However, as shown by Fig.

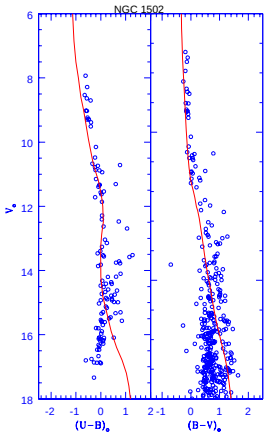

Figure 8. V_o/(U-B)$_o$ and V_o/(B-V)$_o$ CMD of stars lying within the cluster region of the cluster NGC 1502. Solid line is the Schmidt-Kaler (1982) shifted by distance modulus of 10.10 mag.

13, CMD of the cluster NGC 1502 shows significantly large number of stars between the same age spread. We therefore suggest that NGC 1502 emerges as a potential candidate for the study of PMS population.

3.3 Reddening

The reddening, E(B-V) in the cluster region is determined using the (U-B) versus (B-V) colour-colour diagrams (see Figs. 5c, 7c, and 9c). We adopt the slope of the reddening vector E(U-B)/E(B-V) = 0.72 and fit the intrinsic zero-age-main sequence (ZAMS) with solar metallicity Z = 0.019 (Schmidt-Kaler 1982) for main-sequence stars, by shifting the color excesses along the reddening vector. The data show spread in the observed sequence. This infers differential reddening within the cluster region indicating that all three clusters are young. E(B-V) for NGC 2129 varies from 0.68 to 0.85, for NGC 1502 this variation is from 0.58 to 0.78 and for King 12 it is 0.55 to 0.70 which give mean values as 0.77±0.10, 0.68±0.1 and 0.63±0.1 mag respectively as reported in Table 3. The reddening variation for all three clusters is obtained as ~0.2 mag. This value is above the typical width of intrinsic main-sequence stars, i.e., ≤0.11 mag which is usually caused due to photometric accuracy and the presence of binary stars (Sagar 1987). The present values are in agreement with the previously reported ones in the literature.

3.4 Distance and age of the clusters

Distances to the clusters are derived by the ZAMS fitting procedure. Intrinsic CMDs V_o/(B-V)$_o$; V_o/(U-B)$_o$ are plotted. To reduce field star contamination, stars within the cluster radius (r_c)

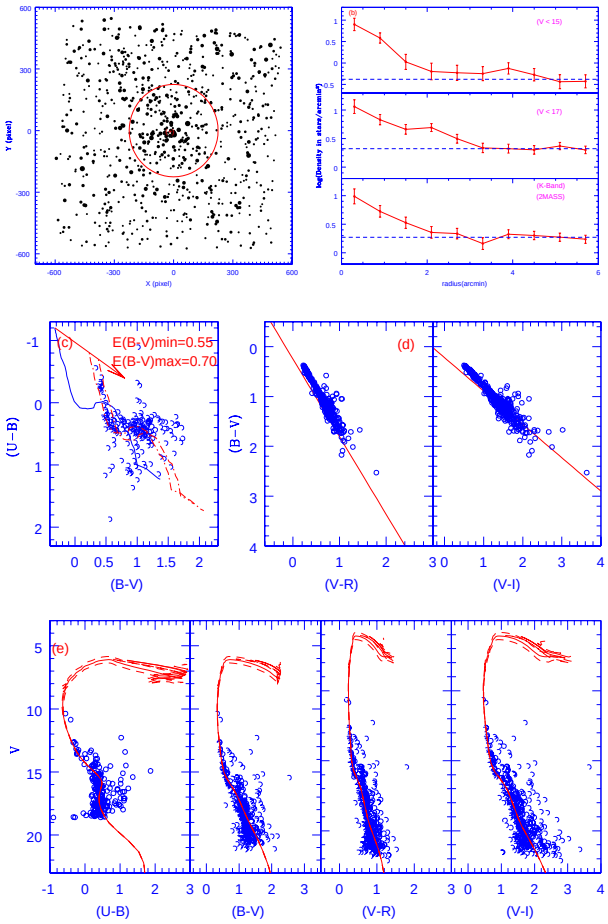

Figure 9. King 12: (a) Identification chart for the observed region of King 12. Filled circles represent apparent magnitude such that brighter stars have larger sizes. The ring defines the cluster boundary. (b) Surface density of stars around the cluster center. Poisson errors are shown with vertical bars. (c) The color-color diagram for the cluster region ($r < r_c$). The (U-B) versus (B-V) diagrams of the stars in cluster region. Continuous straight line represents slope of the reddening vector. Solid line is the Schmidt-Kaler (1982) empirical ZAMS, whereas the dashed lines are the same ZAMS, but shifted by E(B-V) = 0.55 and 0.70 respectively. (d) It shows (V-R)/(B-V) and (V-I)/(B-V) color-color diagram for stars taken within cluster region. The straight line shows least-square fit to the data. (e) The CMDs for the cluster region ($r < r_c$). Isochrones from Girardi et al. (2002) confining the best age estimations are shown by dashed and solid continuous curve for log(age) = 6.95, 7.00 and 7.05.

from the cluster centres have been taken. For plotting these diagrams; apparent V magnitude and (U-B), (B-V) colours have been converted into the intrinsic magnitudes using the mean E(B-V)

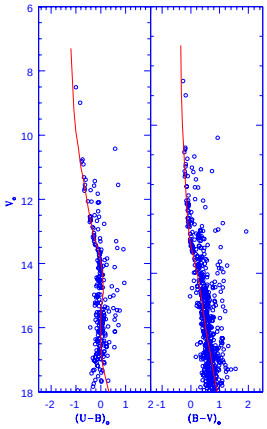

Figure 10. V_o/(U-B)$_o$ and V_o/(B-V)$_o$ CMD of stars lying within the cluster region of the cluster King12. Solid line is the Schmidt-Kaler (1982) shifted by distance modulus of 12.00 mag.

Table 3. The values of E(B-V)max, E(B-V)min and Δ E(B-V).

Cluster	E(B-V)max (mag)	E(B-V)min (mag)	ΔE(B-V) (mag)
NGC 2129	0.85	0.68	0.77
NGC 1502	0.78	0.58	0.68
King 12	0.70	0.55	0.63

value. The following relations (Kamp (1974); Sagar & Joshi (1979); Yadav & Sagar (2002)) for E(U-B) and the absorption A_v towards the cluster in the V band are given by :

E(U-B) = [X + 0.05 E(B-V)] E(B-V)

where X = 0.62 - 0.3 (B-V)$_o$ for (B-V)$_o$ < -0.09

and

X = 0.66 + 0.08 (B-V)$_o$ for (B-V)$_o$ > -0.09

$A_v = R_v$ E(B-V)

where R_v is the ratio of the total-to-selective absorption. We adopt R_v = 3.1 for all three clusters. The Schmidt-Kaler (1982) ZAMS is used to fit in V_o, (U-B)$_o$ and V_o, (B-V)$_o$ color-magnitude diagrams. The visual fit of the ZAMS to the blue part of the intrinsic CMDs gives intrinsic distance modulus (m-M)$_o$. Uncertainties are estimated using the method given by Phelps & Janes (1994).

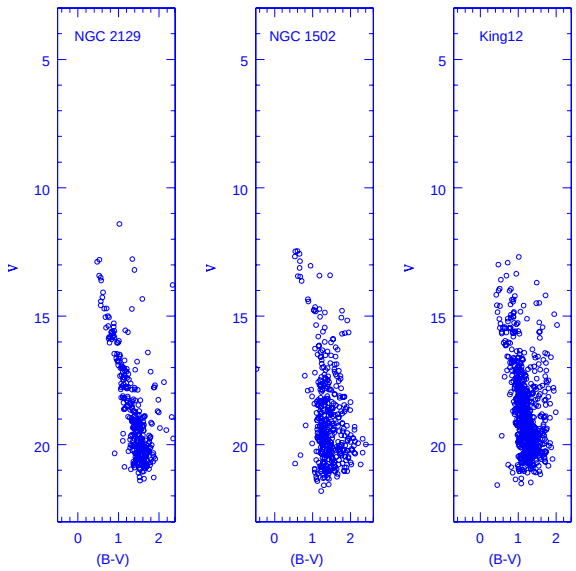

Figure 11. V/(B-V) CMDs for stars outside the cluster region (r ¿ r_c), i.e., field region for NGC 2129, NGC 1502 and King12.

NGC 2129: We show the fitting of ZAMS to V_o, $(U-B)_o$; V_o, $(B-V)_o$, CMDs using mean reddening and the normal extinction law in Fig 6. Stars within the cluster radius has been taken. The inferred true distance modulus $(m-M)_o$ = 11.65 ± 0.15 mag provides a distance of 2137 ± 97pc. This estimate is lower than the value in Table 1.

NGC 1502: The ZAMS fitting for this cluster is shown in the Fig 8. This fitting provides an absolute distance modulus $(m-M)_o$ = 10.10 ± 0.15 mag which gives distance of this cluster as 1047 ± 115pc. This is approximately same as reported by Dias et al. (2002).

King 12: This cluster is best fit for the distance modulus $(m-M)_o$=12.00 ± 0.15 mag giving distance to be 2511 ± 50pc as shown in Fig. 10. This value is slightly high in comparison with the value given in Table 1.

The age of the clusters NGC 2129, NGC 1502 and King 12 have been determined by fitting the theoretical stellar evolutionary isochrones given by Girardi et al. (2002) for solar metallicity Z = 0.019 in the corresponding CMDs (Figs. 5e, 7e and 9e). Theoretical isochrones visually fitted to the main-sequence and brighter stars, i.e, to the bluest envelope of the CMDs indicate log(age) of 6.95, 7.00 and 7.05 after correcting for mean reddening. These are shown by dashed lines for log(age) of 6.95 and 7.05 in the CMDs. Log(age) of 7.00 is shown by solid line which gives an average age of 10 Myr. Using visual fit method, the present data finds the age of all three clusters

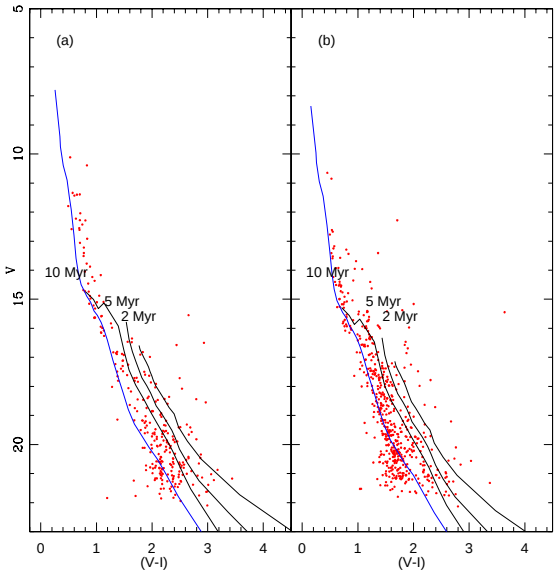

Figure 12. (a) and (b) are V/(V-I) CMDs for stars lying within the cluster region ($r \leq r_c$) for NGC 2129 and King 12. The solid line is ZAMS by Schmidt-Kaler (1982). PMS isochrones for ages 10 Myr, 5 Myr and 2 Myr are plotted using the data by Siess et al. (2000). All the isochrones are corrected for corresponding cluster distance and reddening.

to lie between 8.9 and 11.2 Myr. Thus, we assign an average age of (10.0±0.1) Myr to all of these clusters.

4. Results

Using UBVRI CCD data, the results of our analysis are as follows:

1. The radii of the clusters obtained using radial density profiles are 3.3, 3.7 and 2.7 arcmin which corresponds to 3.3, 1.7 and 3.9 pc for NGC 2129, NGC 1502 and King 12.

2. From the three colour-colour diagrams, we estimated reddening E(B-V) to be 0.77±0.05 mag, 0.68±0.05 mag and 0.63±0.05 mag for the three clusters respectively. The analysis infers differential reddening towards the direction of the clusters.

3. The distances of the three open clusters NGC 2129, NGC 1502 and King 12 have been determined to be 2.1±0.1, 1.0±0.1 and 2.5±0.1 kpc, respectively.

4. An age of 10.0±0.1 Myr has been obtained for all the three clusters by comparing the

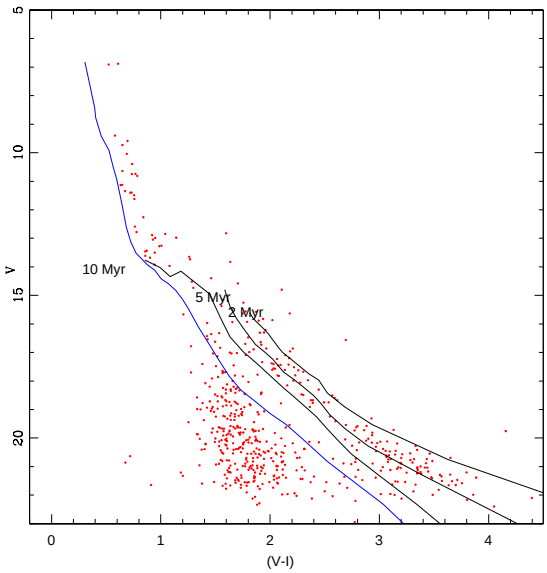

Figure 13. V/(V-I) CMD for stars lying within the cluster region ($r < r_c$) of NGC 1502. The solid line is ZAMS by Schmidt-Kaler (1982). PMS isochrones for ages 10 Myr, 5 Myr and 2 Myr are also plotted using the data by Siess et al. (2000). All the isochrones are corrected for the cluster distance and reddening.

isochrones of solar metallicity Z = 0.019 given by Girardi et al. (2002). CMD for stars lying within the region $r < r_c$ for the cluster NGC 1502 suggests that this open cluster is a probable sight for studying PMS population.

Selected OCs have similar ages indicating their common origin. NGC 2129 is located 2.1 kpc from the Sun in the anti-center direction inside the local spiral arm where the density of OCs is high. Similar environments to the clusters NGC 1502 and King 12 may also be taken. It is to be noted that similar radii, distances and reddening law of selected OCs indicate their origin from similar molecular clouds. It is worth mentioning that more than one star cluster is expected to form from the same parent cloud before it disrupts (Bhatia (1990); Subramaniam et al. (1995)). Thus, studies of a fairly large number of such OCs may provide useful insights towards understanding the evolutionary processes.

Acknowledgments

Authors are thankful to UGC, New Delhi for a Major Research Project vide F No 34-1/2008(SR) dated 31.12.2008 for financial support. This paper is based on observations made at Aryabhatta Research Institute of Observational Sciences (ARIES). We are much thankful to Prof. Ram Sagar, the Director, ARIES, Nainital for providing us local hospitality and other support during our stay

for procuring the observations. We are also thankful to Dr. R. K. S. Yadav for cooperation and useful discussions. We are also grateful to the anonymous referee for constructive suggestions which improved the paper significantly. We are also much obliged for the use of the NASA Astrophysics Data System of SIMBAD data base and the WEBDA open cluster data base.

References

Bhatia R. K., 1990, PASJ, 42, 757
Carraro G., Chaboyer B., Perencevich J., 2006, MNRAS, 365, 867
Crawford D. L., 1994, PASP, 106, 397
Delgado A. J., Alfaro E. J., Garcia-Pelayo J. M., Garrido R., 1992, AJ, 103, 891
Dias W. S., Alessi B. S., Moitinho A., Lépine J. R. D., 2002, A&A, 389, 871
Girardi L., Bertelli G., Bressan A., Chiosi C., Groenewegen M. A. T., Marigo P., Salasnich B., Weiss A., 2002, A&A, 391, 195
Haug U., 1970, A&AS, 1, 35
Hoag A. A., Johnson H. L., Iriarte B., Mitchell R. I., Hallam K. L., Sharpless S., 1961, Publications of the U.S. Naval Observatory Second Series, 17, 343
Kamp L. W., 1974, A&AS, 16, 1
Landolt A. U., 1992, AJ, 104, 340
Mohan V., Pandey A. K., 1984, Ap&SS, 105, 315
Phelps R. L., Janes K. A., 1994, ApJS, 90, 31
Purgathofer A., 1961, ZAp, 52, 186
Reimann H.-G., Pfau W., 1987, Astronomische Nachrichten, 308, 111
Sagar R., 1987, MNRAS, 228, 483
Sagar R., Joshi U. C., 1979, Ap&SS, 66, 3
Schmidt-Kaler T., 1982, Physical parameters of the stars, in Landolt-Bornstein New Series,Vol 2b, Astronomy and Astrophysics/Stars and Star Clusters, eds, K Schaifers & H. H. Voigt, (New York: Springer-Verlag), p. 19
Siess L., Dufour E., Forestini M., 2000, A&A, 358, 593
Stetson P. B., 1987, PASP, 99, 191
Stetson P. B., 1992, in Worrall D. M., Biemesderfer C., Barnes J., eds, Astronomical Data Analysis Software and Systems I Vol. 25 of Astronomical Society of the Pacific Conference Series, More Experiments with DAOPHOT II and WF/PC Images. p. 297
Stetson P. B., 2000, PASP, 112, 925
Subramaniam A., Bhatt B. C., 2007, MNRAS, 377, 829
Subramaniam A., Carraro G., Janes K. A., 2010, MNRAS, 404, 1385
Subramaniam A., Gorti U., Sagar R., Bhatt H. C., 1995, A&A, 302, 86
Tapia M., Costero R., Echevarria J., Roth M., 1991, MNRAS, 253, 649
Yadav R. K. S., Kumar B., Subramaniam A., Sagar R., Mathew B., 2008, MNRAS, 390, 985
Yadav R. K. S., Sagar R., 2002, MNRAS, 337, 133